2014 AIChE R. H. Wilhelm Award in Chemical Reaction Engineering

Adsorption of Nitrogen- and Sulfur-Containing Compounds on NiMoS for Hydrotreating Reactions: A DFT and vdW-Corrected Study

Srinivas Rangarajan and Manos Mavrikakis
Dept. of Chemical and Biological Engineering, University of Wisconsin-Madison, Madison, WI 53706

DOI 10.1002/aic.15025
Published online September 17, 2015 in Wiley Online Library (wileyonlinelibrary.com)

Adsorption of 35 molecules, comprising of organonitrogen and organosulfur compounds and hydrocarbons relevant to hydrotreating, was studied on the nickel-promoted metal edge of molybdenum sulfide catalysts using periodic DFT, accounting for van der Waals interactions in several cases. Basic molecules tend to adsorb via their nitrogen atoms directly on top of nickel atoms while nonbasic molecules adsorb via carbon atoms relatively weakly. Molecular size, electron density, and alkyl substitution affects binding at the GGA-PW91 level of theory. van der Waals corrections influence adsorption geometry and lead to significant additional stabilization of adsorbates. The differential binding energy of nitrogen-containing compounds decreases by 0.2–0.3 eV for each additional molecule added on the edge and their presence destabilizes the binding of organosulfur compounds by more than 0.2 eV. The inhibition of hydrodesulfurization is suggested to arise from site blocking and destabilization of reaction intermediates and transition states by organonitrogen compounds. © 2015 American Institute of Chemical Engineers *AIChE J*, 61: 4036–4050, 2015
Keywords: adsorption/gas, adsorption/liquid, computational chemistry (at solid surfaces), computational chemistry (kinetics/thermo), computational chemistry (quantum chemistry), hydrodesulfurization, nitrogen inhibition

Introduction

Increasingly stringent emission standards, especially on sulfur content in diesel which is required to be less than 15 ppm in several countries including the United States, have led to the development of deep desulfurization catalysts and processes that can remove sulfur, in a hydrotreating step, from compounds such as alkyl substituted dibenzothiophenes in gas oil fractions.[1,2] Hydrotreating in general, and hydrodesulfurization (HDS) in specific, is industrially carried out on promoted (nickel or cobalt) molybdenum sulfide (MoS_2) catalysts (nickel promoted molybdenum sulfide [NiMoS] or cobalt promoted molybdenum sulfide [CoMoS]). Experimental, specifically spectroscopy and microscopy,[3–7] and theoretical studies[8–10] have together shown that: (a) the active sites are located at or near the two types of edges—"metal" and "sulfur" edges—of the layered molybdenum disulfide particles,[11–15] (b) these edges can be decorated by sulfur atoms, sulfur dimers, and sulfohydryl (—SH) groups, under reaction conditions,[16–25] (c) sites with sulfur unsaturation, referred to as coordinatively unsaturated sites, are active for HDS,[13,15,26,27] (d) "brim" sites near the edges and above the MoS_2 layer can be potential alternative sites for HDS,[23,25,28] (e) cobalt and nickel promoter atoms replace the edge molybdenum atoms partially or completely, with cobalt preferring the sulfur edge while nickel substitutes molybdenum at the metal edge,[29–32] and (f) support interactions with the catalyst can affect the morphological characteristics such as shape, size, and orientation, the electron density, and the activity of the catalyst.[28,33–36]

Under reaction conditions, the organonitrogen compounds in gas oil can adsorb and undergo hydrodenitrogenation (HDN)[1,37] on these catalysts and thereby inhibit HDS.[38] Several experimental studies have been reported focusing on the effect of nitrogen-containing compounds on sulfur removal with model and industrial feeds.[39–42] Reaction inhibition studies have been used to calculate effective adsorption constants of various nitrogen-containing compounds on the catalyst assuming simple reaction models such as Langmuir–Hinshelwood expressions. Comparatively, very few theoretical studies have focused on inhibition effects of organonitrogen compounds on industrial catalysts. Specifically, Sun et al. calculated the binding energies of few basic and nonbasic heavy organonitrogen compounds, such as acridine and carbazole, and adsorption constants (temperature-corrected) of compounds, such as pyridine, aniline, and ammonia, on NiMoS

Additional Supporting Information may be found in the online version of this article.

Correspondence concerning this article should be addressed to M. Mavrikakis at emavrikakis@wisc.edu.

using density functional theory (DFT).[43–45] The exact nature and strength of adsorption of nitrogen-containing compounds vis-à-vis sulfur-containing molecules and their mechanism of inhibition of HDS, however, remains largely unexplored.

In this work, we use density functional theory accounting for van der Waals (vdW) dispersive interactions to study the adsorption of a comprehensive set of molecules relevant in HDS and HDN on the nickel-promoted metal edge of NiMoS. Specifically, we consider a total of 35 compounds comprising of basic and nonbasic aromatic organonitrogen compounds and their alkyl substituted forms (e.g., pyridine, aniline, pyrrole, indole, and dimethyl acridine), organosulfur compounds (thiophene, dibenzothiophene, etc.), hydrocarbons such as small alkanes, olefins, and aromatics (benzene, naphthalene), and small molecules such as hydrogen, ammonia, and hydrogen sulfide. We begin with a description of our computational methods. The results of these calculations are presented subsequently. We further present: (1) calculated temperature-dependent adsorption constants for a subset of these compounds and compare these numbers with experimentally determined inhibition constants, (2) adsorption of nitrogen-containing compounds at high surface concentrations, and (3) coadsorption of organonitrogen and organosulfur compounds. Using this large dataset which is diverse in terms of molecules and coverages, we discuss an emerging picture of inhibition by organonitrogen compounds in terms of site blocking and adsorbate destabilization and relate experimental trends in HDN, HDS, and inhibition by nitrogen-containing compounds to our results.

Computational Methods

The catalyst model was chosen on the basis of experimental information on the bulk MoS_2 and catalyst particles. MoS_2 is a layered transition metal dichalcogenide with each layer consisting of a trilayer "S-Mo-S" sandwich with molybdenum atoms occupying a trigonal prismatic position and coordinated to six sulfur atoms. The layers are held to each other by weak van der Waals forces and the number of layers in a catalyst particle depends on the nature of the support, synthesis protocol and reaction conditions, and promoter concentration. Transmission electron microscopy studies have shown that NiMoS particles can be synthesized on alumina supports such that they contain one or two layers of catalyst.[35,46] Further, catalyst particles expose two types of edges based on their termination. *Ab initio* studies have shown that the most preferred nickel promoted edge morphology is a metal edge with complete replacement of edge molybdenum atoms by nickel and no further decoration by sulfur leading to a square planar geometry around the nickel atoms[31,47]; this edge has been proposed to be the location of active sites in NiMoS.

An infinite "stripe" model consisting of a single layer of four rows of six metal atoms, with nickel occupying the top rows was used to represent the catalyst in our calculations; see Figure 1. The axes of the model are marked in Figure 1 but have been dropped in subsequent figures; the front view of the model (top right) is along the z direction, side view (top left) along the y axis, and the top view (bottom right) along the negative x axis. The system is periodically repeated in the y direction and sufficient vacuum (of greater than 10 Å upon the adsorption of the largest molecule studied herein—benzocarbazole) is used in the x and z directions resulting in a supercell size of 27 Å × 19.14 Å × 22.5 Å. The plane wave density functional theory code VASP[48,49] is used for all calculations. A Monkhorst-Pack k-point set of 1 × 2 × 1 is used to sample

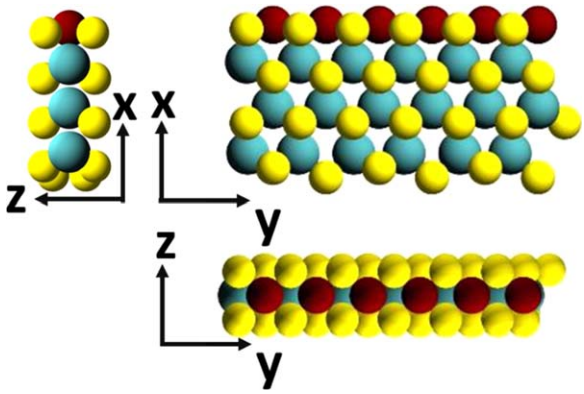

Figure 1. NiMoS catalyst single layer stripe model periodic along *y* axis.

Red: nickel, cyan: molybdenuym, and yellow: sulfur. [Color figure can be viewed in the online issue, which is available at wileyonlinelibrary.com.]

the Brillouin zone.[50] Generalized gradient corrected PAW potentials[51] are used for all atoms and PW91[52,53] is used as the exchange correlation functional in non-vdW calculations (referred to henceforth as GGA-PW91). A Gaussian smearing width of 0.05 eV is used for all calculations and the energies are extrapolated to 0 K. A plane wave cutoff of 400 eV and a density wave cutoff of 640 eV was used in all calculations. The convergence criterion for geometric relaxation was 0.02 eV/Å. All calculations were spin polarized, with dipole corrections included, and all atoms were relaxed. The lattice constant calculated using the PW91 functional is 3.19 Å which compares well with the experimental value of 3.16 Å.[54] In some cases, two adjacent slab models were also considered for comparison. In these cases, the MoS_2 interlayer (Mo-Mo) distance was fixed at 6.3 Å as calculated using PW91; this is close to the experimental value of 6.15 Å.[54,55] A vdW-DF-based method, specifically optB86b-vdW,[56,57] is used to account for nonlocal van der Waal's (vdW) corrections while all other parameters are fixed as above. The lattice constant calculated with this method is 3.17 Å. Gas-phase calculations are carried out at the same level of theory as the slab calculations, in a cell that allows for at least 10 Å of vacuum between atoms in adjacent cells even for the largest molecule considered (corresponding to a cell dimensions of 30 × 30.5 × 31 Å). To rigorously probe combinations of adsorption geometry and sites, a number of adsorption structures were studied for each adsorbate molecule. Specifically, we consider adsorption modes: (a) with the plane containing the adsorbates being perpendicular or parallel to the length of the edge (y axis), (b) such that the adsorbate is in an upright, slanted, or flat geometry with respect to the width of the edge (plane of the adsorbate perpendicular, at an angle, or parallel to the y-z plane), and (c) with adsorbate atoms atop nickel atoms, on the bridge between two nickel atoms, or on the brim. We report only the most stable structure and the respective energetics for each molecule.

The binding energy of a molecule is calculated as

$$\mathrm{BE} = \Delta E_{\mathrm{binding}} = E_{\mathrm{molecule+slab}} - E_{\mathrm{molecule,gas}} - E_{\mathrm{slab}} \qquad (1)$$

The entropies and enthalpies of adsorption at different temperatures are obtained from vibrational frequency calculations and statistical mechanical equations.[58] The entropy of a molecule, adsorbed or gaseous, can be written as the sum of contributions from rotational, translational, and vibrational degrees of freedom

Table 1. Binding Energies of Molecules on NiMoS Using GGA-PW91 and optB86b-vdW Methods: Values in Parentheses are for Adsorption in a Parallel Upright Configuration when Perpendicular Upright Configuration is the Most Stable

	Binding Energy (eV)		
Compound	GGA-PW91	optB86b-vdW	Literature
H_2	−0.22	−0.18	−0.21[59]
H_2S	−0.80	−0.97	−0.82[59]
NH_3	−1.17	−1.29	−1.26[44]
C_2H_6	−0.11	−0.29	
C_2H_4	−0.73	−0.97	
Benzene	−0.28		
Tolouene	−0.34		
Aniline	−1.00	−1.47	−1.4[44]
Pyridine	−1.17 (−1.05)	−1.50 (−1.43)	−1.3[45]
2-Methylpyridine	−1.10 (−0.87)		
Lutidine	−0.76 (−0.26)	−1.21 (−0.82)	
Quinoline	−1.10 (−0.81)	−1.51 (−1.26)	−1.13[43]
2,8 Dimethylquinolone	−0.37		
Acridine	−0.79 (−0.44)	−1.45	−0.82[43]
Dimethylacridine	−0.41		
Diethylacridine	−0.45		
Dipropylacridine	−0.46		
2-Methylacridine	−0.82		
3-Methylacridine	−0.83		
4-Methylacridine	−0.37		
9-Methylacridine	−0.67		
4-Ethylacridine	−0.43		
4-Propylacridine	−0.46		
Pyrrole	−0.65	−1.11	−0.71[43]
2,5 Dimethylpyrrole	−0.66		
Indole	−0.66	−1.33	−0.81[43]
Carbazole	−0.45	−1.34	−0.57[43]
Dimethylcarbazole	−0.51		
Benzocarbazole	−0.47		
Thiophene	−0.60	−1.06	−0.49[44]
Benzothiophene	−0.69		
Dibenzothiophene	−0.79	−1.52	
4-Methyldibenzothiophene	−0.78		
4,6-Dimethyldibenzothiophene	−0.71	−1.52	
Naphthalene	−0.40		

$$S_{\text{total}} = S_{\text{rot}} + S_{\text{trans}} + S_{\text{vib}} \tag{2}$$

The vibrational entropy contribution can be calculated from the frequency values, ϑ_i, as

$$S_{\text{vib}} = k_B \sum_{i}^{\#\text{ modes}} \left(\frac{x_i}{e^{x_i} - 1} - \ln\left(1 - e^{-x_i}\right) \right) \tag{3}$$

$$x_i = \frac{h\vartheta_i}{k_B T} \tag{4}$$

The rotational and translational components of entropy for gaseous species are calculated using the ideal gas assumption and standard statistical mechanics equations. For a surface intermediate, the smallest vibrational mode is assumed to be translational along the edge and treated as a mobile adsorbate with full one-dimensional (1-D) translational entropy; this assumption represents the upper bound on the translational entropy contribution. The lowest mode, therefore, is separated before diagonalizing the Hessian matrix. The rotational modes are assumed to be frustrated vibrational modes and are calculated using Eqs. 3 and 4. The 1-D translational entropy is calculated (in a manner similar to three-dimensional and two-dimensional entropy terms) as

$$S_{\text{trans,1-D}} = R\left(\log\left(\frac{\sqrt{2\pi mkT}}{h} \right) - \log\left(C_0\right) + 1.5 \right) \tag{5}$$

where C_0 is the surface concentration at saturation on the edge. For this study, we assume saturation corresponds to one-to-one ratio of adsorbate and nickel atoms; C_0 is, therefore, taken to be the reciprocal of the lattice constant.

The enthalpy of adsorption is calculated as

$$\Delta H(T) = \Delta E + \text{ZPE} + \int C_P(T)\,dT \tag{6}$$

where ZPE is the zero point energy correction calculated from computed vibrational frequencies. Shomate equations were fit to entropy values at different temperatures, from which the heat capacity at constant pressure, C_P, is calculated. The specific temperature dependent expressions are given in Supporting Information.

Results

Table 1 contains the binding energies of all adsorbates on NiMoS, considered in this study, calculated using GGA-PW91 and optB86b-vdW functionals, and lists comparisons with literature wherever available. All literature values do not account for van der Waals corrections; the binding energies calculated in this work at the GGA-PW91 level of theory match the literature within 0.2 eV in most cases except for aniline wherein the difference is 0.4 eV likely owing to the differences in the computational code used and the basis sets adopted, even

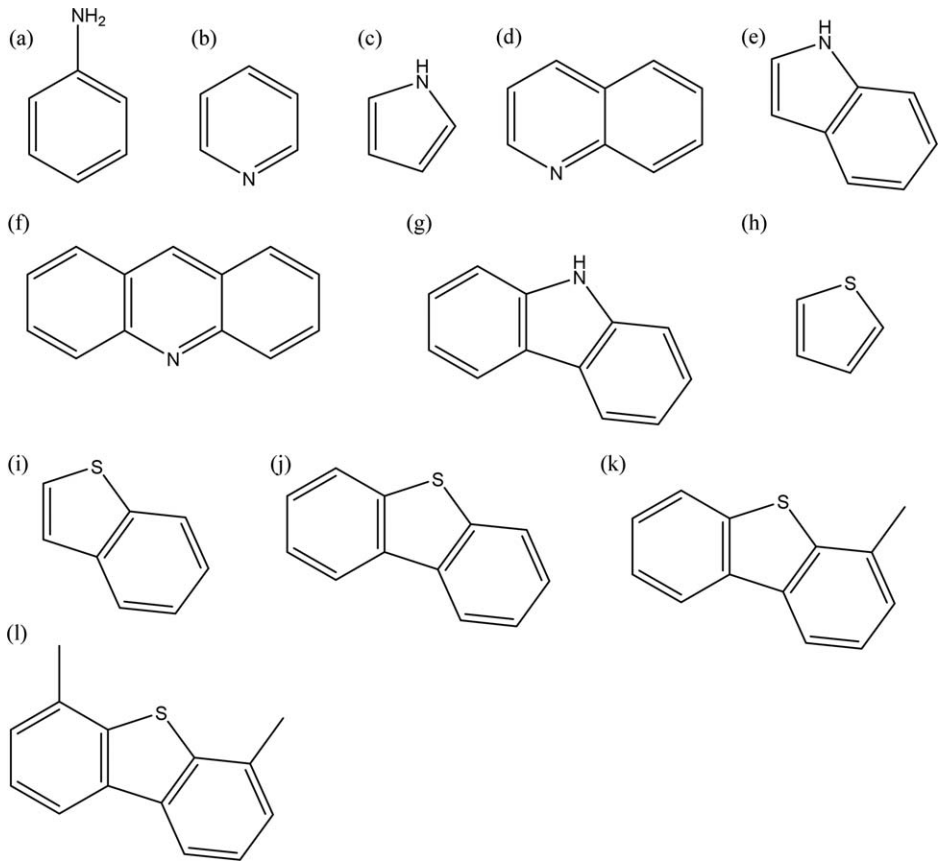

Figure 2. Organonitrogen and organosulfur compounds in this study: (a) aniline, (b) pyridine, (c) pyrrole, (d) quinoline, (e) indole, (f) acridine, (g) carbazole, (h) thiophene, (i) benzothiophene, (j) dibenzothiophene, (k) 4-methyldibenzothiophene, and (l) 4,6 dimethyldibenzothiophene.

Alkyl substituted organonitrogen compounds are given in Supporting Information S2.

though the adsorption structures in both cases are similar. The van der Waal's corrected values for binding energies have been calculated only for a subset of all compounds studied herein in view of the higher computational cost. Specifically, van der Waal's corrected values were not calculated for alkyl substituted organonitrogen and all aromatic compounds. The Supporting Information S1 contains the Ni—N or Ni—C atomic distance values between the nickel atom of the edge and the atom through which the organonitrogen compounds bind. The basic and nonbasic unsubstituted organonitrogen compounds and all organosulfur compounds considered in this study are presented in Figure 2; alkyl substituted organonitrogen compounds considered in this study are given in the Supporting Information S2. The binding energies depend on a variety of factors including molecular size, electron density, steric hindrance, basicity, and substitution; the adsorption characteristics of different classes of compounds are discussed in detail below. We begin our analysis with binding energy values calculated at the GGA-PW91 level of theory; unless otherwise stated, the reported energetics are based on the GGA-PW91 exchange-correlation functional.

Basic nitrogen compounds

Figure 3 shows the best adsorption structures for ammonia, aniline, pyridine, quinoline, and acridine. We predict perpendicular adsorption modes for heteroaromatic molecules with the molecules being upright, or slightly tilted to increase the distance between carbon or hydrogen atoms adjacent to nitrogen and the nickel edge. Aniline, on the other hand, is slanted in accordance with the tetrahedral hybridization on the nitrogen atom, which is also the case for the nitrogen atom in ammonia. Adsorption is, in all cases, via the nitrogen atom and the size of the molecule affects the binding energy; specifically, the relative stability (energy difference) of perpendicular upright structures over parallel upright structures increases as pyridine $<$ quinoline $<$ acridine, clearly indicating the steric effect of aromatic rings in the latter two molecules. Further, Ni—N atomic distance correlates with adsorption strength across heteroaromatic and nonaromatic nitrogen-containing compounds (see Supporting Information S1 for these distances).

Effect of Alkyl Substitution. Table 1 contains the calculated binding energies for 2-methylpyridine, lutidine (2,6 dimethylpyridine), 2,8-dimethylquinoline, 2-,3-,4-,9-methylacridines, 4-ethylacridine, 4-propylacridine, and di-methyl/ethyl/propylacridines (molecular structures of these molecules and the preferred adsorption structures are given in Supporting Information S2). For substituted pyridine, monosubstitution does not lead to any destabilization in the perpendicular adsorption mode while dimethyl substitution (lutidine) leads to a significant destabilization of about 0.3 eV (see structure in Figure 4) due to steric hindrance by the substituents.

The location of the monomethyl substitution can play a significant role in acridine. While methyl substitution at the position closest to nitrogen (4-methyl acridine) results in significant destabilization (0.3 eV, see structure in Figure 4)

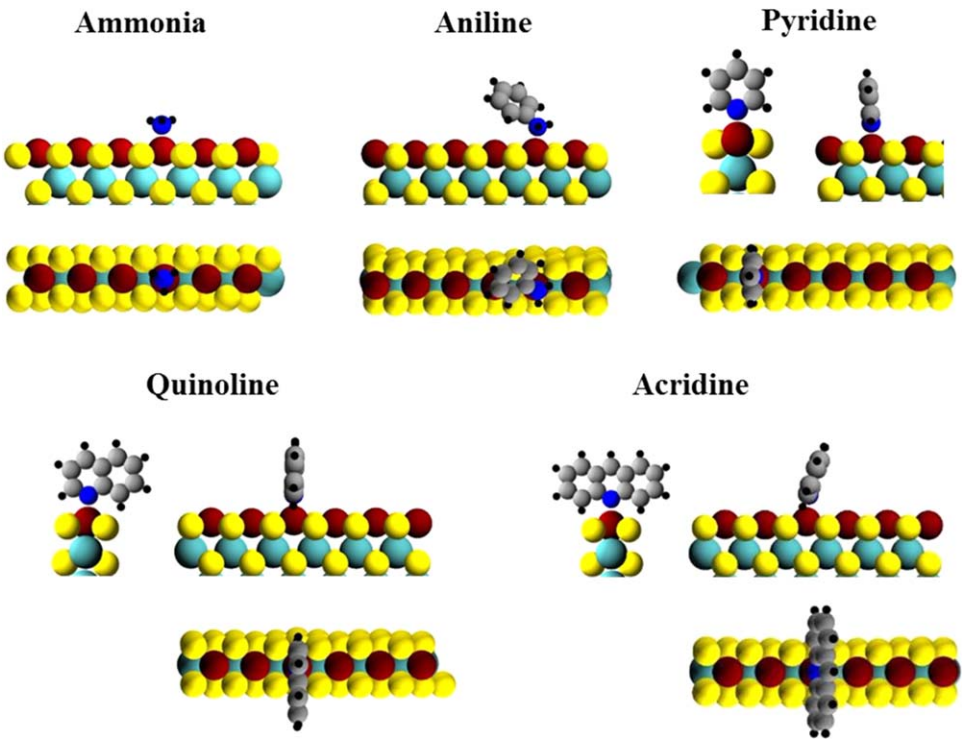

Figure 3. Most stable GGA-PW91 adsorption structure for ammonia, aniline, pyridine, quinoline, and acridine.

Red: nickel, yellow: sulfur, cyan: molybdenum, black: hydrogen, gray: carbon, and blue: nitrogen. [Color figure can be viewed in the online issue, which is available at wileyonlinelibrary.com.]

because of steric hindrance, the other positions do not affect adsorption appreciably. Further, the effect of increasing the size of the alkyl group is also minimal as 4-ethyl and 4-propyl acridines have the same binding energy values as 4-methylacridine. Upon adding a second alkyl group, to obtain dimethyl, diethyl, or dipropyl acridine, the binding energy does not change appreciably relative to 4-methyl acridine (dimethyl acridine shown in Figure 4). The adsorption structure of hindered acridines is similar—they bind via the aromatic ring rather than the nitrogen atom. Dimethyl quinoline too prefers to adsorb in a flat configuration via its aromatic rings (see figure in Supporting Information S2).

Effect of Including a Second Slab in the Calculations. As noted earlier, stacking of NiMoS slabs can occur in real catalysts and, therefore, the effect of a second slab may be significant. Furthermore, pyridine, quinoline, and acridine tend to adsorb perpendicular to the slab in a single slab calculation. To test the effect of additional layers, calculations with a two-layer catalyst model were carried out and are presented in Supporting Information S3. The binding energies are slightly lower due to repulsive electronic interactions with the second slab but are within 0.15 eV even for acridine; the most stable adsorption structure remains upright and perpendicular when using the GGA-PW91 functional.

Nonbasic nitrogen-containing compounds

Table 1 reports binding energy values of nonbasic nitrogen molecules such as pyrrole, indole, and carbazole. We note that: (a) their binding energies are significantly lower than those for basic nitrogen compounds containing the same

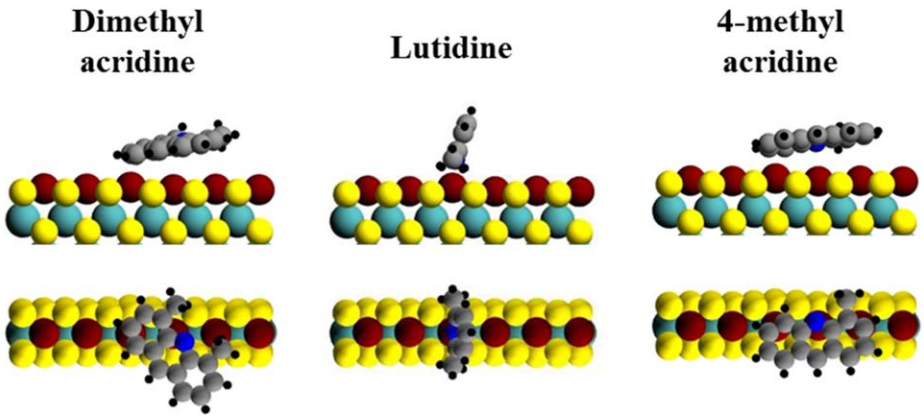

Figure 4. Most stable GGA-PW91 adsorption structure of dimethyl acridine (left), lutidine (middle), and 4-methyl acridine (right).

Red: nickel, yellow: sulfur, cyan: molybdenum, black: hydrogen, gray: carbon, and blue: nitrogen. [Color figure can be viewed in the online issue, which is available at wileyonlinelibrary.com.]

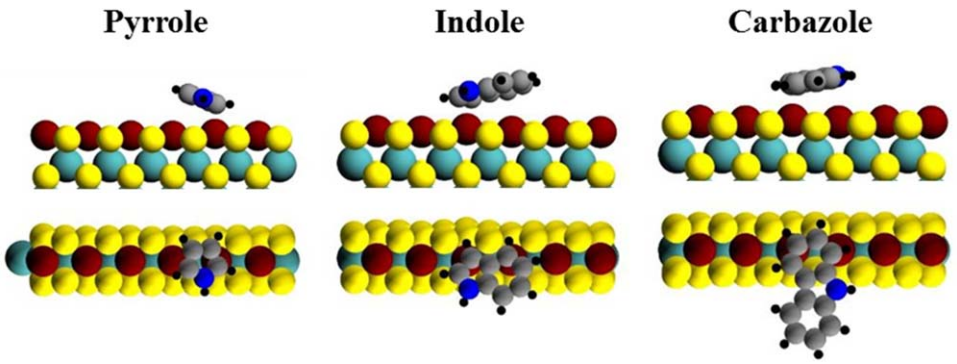

Figure 5. Most stable GGA-PW91 adsorption structure of pyrrole, indole, and carbazole on NiMoS.

Red: nickel, yellow: sulfur, cyan: molybdenum, black: hydrogen, gray: carbon, and blue: nitrogen. [Color figure can be viewed in the online issue, which is available at wileyonlinelibrary.com.]

number of rings (pyridine, quinoline, and acridine, respectively), (b) the adsorption is through aromatic carbon atoms (Figure 5), and (c) the molecules adsorb flat in either a parallel (indole) or perpendicular (carbazole) configuration as seen in Figure 5. For pyrrole and indole, the adsorption is through the carbon atoms on the heteroaromatic ring closest to the nitrogen atom, while for carbazole, because heteroaromatic carbon atoms are unavailable, the adsorption is through the carbon atoms on the outer aromatic rings.

Effect of Alkyl Substitution. The effect of alkyl substitution was probed by considering dimethylpyrrole and dimethylcarbazole (adsorption structures shown in Supporting Information S2); while the binding energy of dimethylpyrrole is similar to that of pyrrole, the binding of dimethylcarbazole is slightly stronger than carbazole (by about 0.05 eV), even though the difference is within the typical error of DFT calculations. However, it should be noted that methyl groups increase electron density on the neighboring or the para carbon of the atom having the methyl substitution thereby potentially leading to additional stabilization as observed in our calculations. The adsorption configuration of dimethyl substituted carbazole (not shown) is similar to that of dimethyl acridine, that is flat and at an angle to the edge. Therefore, it is expected that the length of the alkyl chain and the number of substitutions will not significantly alter binding energies of substituted carbazoles as well.

Hydrocarbons

Aromatics. Table 1 reports the GGA-PW91 binding energies of benzene, toluene, and naphthalene. The binding energies are small (−0.3 to −0.4 eV) and there is a small effect of methyl substitution in toluene vis-à-vis benzene (0.05 eV). The adsorption structures are given in Supporting Information S8.

Linear. Ethane and ethylene GGA-PW91 binding energies were calculated, as reported in Table 1. Ethane adsorbs very weakly; ethylene, on the other hand, adsorbs relatively strongly (−0.7 eV). The preferred adsorption structures are given in Supporting Information S8.

Sulfur-containing compounds

Hydrogen Sulfide. Hydrogen sulfide adsorbs as strong as nonbasic compounds with a binding energy of −0.80 eV. The sulfur atom, possessing two lone pairs, directly binds to the nickel atom. The most stable adsorption structure is given in Supporting Information S8.

Thiophene Family of Molecules. Table 1 reports the GGA-PW91 adsorption of thiophene, benzothiophene, dibenzothiophene, 4-methyldibenzothiophene, and 4,6 dimethyldibenzothiophene. We observe that binding energies increase marginally with increasing molecular size, however, there is a mild steric hindrance for the 4,6 dimethyl dibenzothiophene. Figure 6 shows the adsorption structure of thiophene, dibenzothiopehene, 4-methyl dibenzothiophene, and 4,6 dimethyl dibenzothiophene; the most stable adsorption structure is perpendicular to the edge and slanted (30°–60°) toward it.

Adsorption at higher surface concentrations

In this section, we consider adsorption trends at higher surface concentration of molecules. Specifically, we consider the

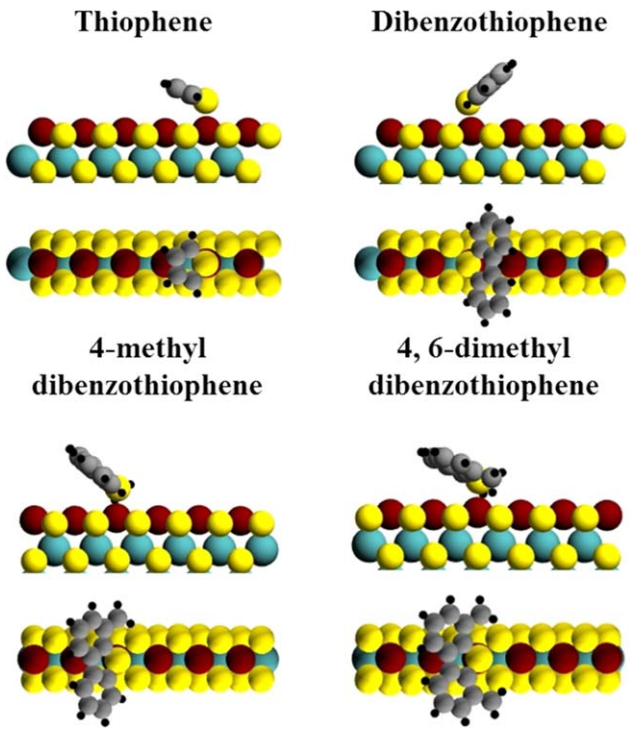

Figure 6. Most stable adsorption structure (GGA-PW91) of heteroaromatic organosulfur compounds.

Red: nickel, yellow: sulfur, cyan: molybdenum, black: hydrogen, gray: carbon, and blue: nitrogen. [Color figure can be viewed in the online issue, which is available at wileyonlinelibrary.com.]

Table 2. Differential GGA-PW91 Binding Energy (and Net Deviations) of Nitrogen-Containing Compounds and Thiophene for Different Values of *n*—the Number of Molecules of that Compound in the Supercell: The Values for $n = 1$ (Reproduced from Table 1) are Given here for Convenience

	$(\Delta E)_n$ [$BE_{net,n}$] (eV)			
Compound	$n = 1$	$n = 2$	$n = 3$	$n = 4$
NH_3	−1.17	−0.85 [0.31]	−0.67 [0.5]	−0.55 [0.62]
Pyridine	−1.17	−0.96 [0.2]	−0.67 [0.48]	−0.44 [0.71]
Aniline	−1.00	−0.75 [0.25]		
Quinoline	−1.10	−0.71 [0.39]		
Lutidine	−0.76	−0.46 [0.3]		
Thiophene	−0.60	−0.42 [0.18]	−0.21 [0.39]	

trend in the binding energy of nitrogen-containing compounds and thiophene as a function of surface concentration (measured herein as the number of molecules per edge Ni atom). It is important to note the distinction between surface coverage and concentration; while concentration is the number of molecules per Ni atom, the coverage is the fraction of area of the active sites occupied by the adsorbate molecules. For example, a flat and parallel adsorption of acridine occupies more than 50% of the edge leading to an effective coverage of 0.5 but having a surface concentration of 0.16 molecules per Ni atom. The effect of higher concentration is measured in terms of differential binding energy $(\Delta E)_n$ of an adsorbate species upon the adsorption of an additional molecule of organonitrogen or organosulfur compound on an edge already bearing $n-1$ of those molecules. Mathematically, it is defined as

$$(\Delta E)_n = E_{n\,\mathrm{mol}} - E_{\mathrm{molecule,gas}} - E_{n-1\,\mathrm{mol}} \tag{7}$$

where $E_{i\,\mathrm{mol}}$ is the total energy the supercell with i identical molecules adsorbed (and $E_{0\ \mathrm{mol}}$ is the total energy of the clean edge). Further, the net deviation in binding energy from the case $n = 1$, $BE_{net,n}$, can be calculated as

$$\mathrm{BE}_{\mathrm{net},n} = (\Delta E)_n - \Delta E_{1\ \mathrm{mol}} \tag{8}$$

Table 2 lists the differential binding energies and net deviation in square brackets of some nitrogen-containing compounds and thiophene for different values of n. Given the computational demands of calculating the binding energies at higher surface concentrations in all cases, we performed calculations for $n = 3$ and $n = 4$ only for ammonia and pyridine. The adsorbates are significantly destabilized at high concentrations. This destabilization can substantially reduce the adsorption constants of molecules at conditions where high surface concentrations become relevant. We note from Table 2 that quinoline has the highest level of destabilization of about 0.4 eV (the net deviation in binding energy value) upon the addition of a second molecule ($n = 2$). Figure 7 shows pyridine adsorption at various values of n as a representative example of adsorption at higher concentrations; in general, adsorbates tend to maximize the distance between each other, when coadsorbed.

Destabilization of thiophene adsorption in the presence of nitrogen-containing compounds

Adsorption of thiophene is affected by the presence of preadsorbed nitrogen-containing compounds. The destabilization energy of thiophene adsorption as a function of n additional molecules of a nitrogen-containing compound is defined as

$$D_{\mathrm{Thiophene}} = \Delta E_{\mathrm{Thiophene}+n\ \mathrm{N\text{-}compound}} - \Delta E_{\ n\ \mathrm{N\text{-}compound}} - \Delta E_{\mathrm{Thiophene}} \tag{9}$$

where $\Delta E_{\mathrm{Thiophene}+n\ \mathrm{N\text{-}compound}}$ is the net binding energy of thiophene and n molecules of a N-containing compound, $\Delta E_{n\ \mathrm{N\text{-}compound}}$ is the binding energy of just the n molecules of that N-containing compound, and $\Delta E_{\mathrm{Thiophene}}$ is the binding energy of thiophene in the absence of coadsorbed molecules of the N-containing compound.

Table 3 shows GGA-PW91 values for thiophene destabilization induced by the presence of different nitrogen-containing compounds. Figure 8 shows adsorption of thiophene at different pyridine concentrations as a representative example of thiophene adsorption in the presence of nitrogen-containing compounds. The coadsorbed molecules tend to maximize the distance between each other, however, the adsorption structures of individual compounds in the coadsorbed states are not significantly different from that of their most stable individually adsorbed states. Supporting Information S9 contains figures showing coadsorption of thiophene and organonitrogen compounds.

Effect of van der Waal's interactions

Basic Organonitrogen Compounds. Table 1 includes the van der Waals corrected binding energies for basic nitrogen compounds. For small compounds (aniline, pyridine, and lutidine), the additional stabilization gained because of vdW effects is of the order of 0.5 eV; a stabilization of 0.1 eV was observed for ammonia. For these compounds, the adsorption structures are similar to those shown in Figure 3, which were obtained by using the GGA-PW91 functional for the energy minimization. For acridine, on the other hand, the net stabilization due to the inclusion of vdW interactions is 0.7 eV and the most stable structure in this case is a flat and parallel

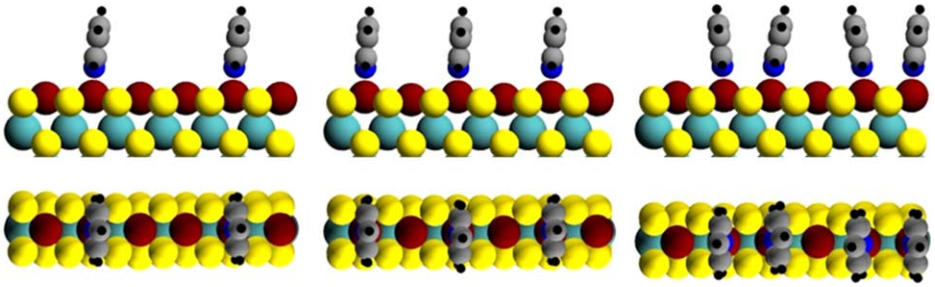

Figure 7. Most stable adsorption structure (GGA-PW91) of two (left), three (middle), and four (right) pyridine molecules on NiMoS.

Red: nickel, yellow: sulfur, cyan: molybdenum, black: hydrogen, gray: carbon, and blue: nitrogen. [Color figure can be viewed in the online issue, which is available at wileyonlinelibrary.com.]

Table 3. Thiophene Destabilization at Different Concentrations of Preadsorbed Nitrogen-Containing Compounds Calculated at the GGA-PW91 Level of Theory: *n* Represents the Number of Preadsorbed N-Containing Molecules

Compound	$D_{\text{Thiophene}}$ (eV)			
$n\rightarrow$	1	2	3	4
Ammonia	0.2	0.37	0.53	
Pyridine	0.19	0.46	0.62	1.11
Aniline	0.22	0.33		
Quinoline	0.27	0.40		
Lutidine	0.23	0.35		
Indole	0.25			
Acridine	0.24			
Carbazole	0.21			

adsorption mode as shown in Figure 9 (right), in contrast to the upright and perpendicular structure obtained using GGA-PW91 (Figure 9 left and Figure 3).

The GGA-PW91 binding energy of the adsorption mode shown in Figure 9 (right) is about 0.4 eV less than the acridine adsorption structure shown in Figure 9 (left), because the binding in the former is via the aromatic ring rather than the nitrogen atom.

Evidently, there is a tradeoff between a "flat-parallel" adsorption mode (Figure 9 right) and "upright-perpendicular" mode (Figure 9 left)—the former allows for more interaction of the atoms in the molecule with the catalyst edge thereby increasing vdW stabilization, while the latter allows for better nickel–nitrogen coordination. The most stable adsorption structure is, therefore, size dependent; as vdW stabilization increases with the number of nonhydrogen atoms, for molecules as large as acridine and larger, vdW effects outweigh electronic factors. vdW-corrected values for acridine and quinoline based on other methods (optPBE, optB88, and DFT-D2) are given in Supporting Information S4; while the absolute values of the binding energies are different, the relative trends are preserved.

Nonbasic Organonitrogen Compounds. Table 1 has the vdW corrected binding energy values of nonbasic organonitrogen compounds. The effect of vdW stabilization is significantly higher for nonbasic compounds, primarily because of the flat adsorption structure and, therefore, a greater level of interaction of carbon/nitrogen atoms with the edge. The additional stabilization increases from 0.5 eV for pyrrole to almost 1 eV in the case of carbazole. While the structure for pyrrole and indole are similar to that obtained without vdW corrections, carbazole prefers to adsorb in a parallel configuration instead of a perpendicular one with respect to the edge (Figure 10 right), much like the case of acridine, thereby increasing its interaction with the edge.

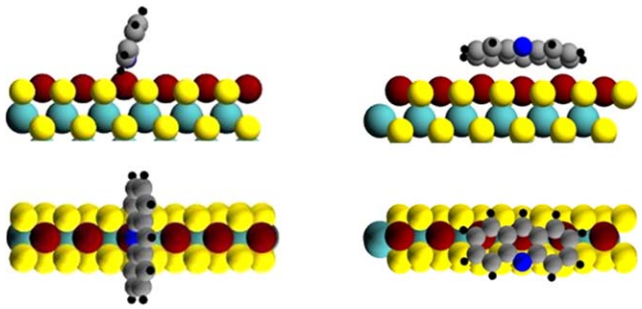

Figure 9. Most stable adsorption structure of acridine at GGA-PW91 (left) and van der Waals corrected optB86b (right) levels of theory.

Red: nickel, yellow: sulfur, cyan: molybdenum, black: hydrogen, gray: carbon, and blue: nitrogen. [Color figure can be viewed in the online issue, which is available at wileyonlinelibrary.com.]

Sulfur-Containing Compounds. The effect of vdW interactions (vdW-corrected values are in Table 1) is significant for thiophenic compounds; an additional stabilization of about 0.2 eV is seen for hydrogen sulfide, while thiophene, dibenzothiophene, and 4,6 dimethyl dibenzothiophene are stabilized by 0.5, 0.7, and 0.8 eV, respectively. The preferred adsorption geometries, interestingly, are not significantly altered in these cases relative to those shown in Figure 6, which were calculated with GGA-PW91.

Hydrocarbons. Ethane is primarily stabilized by vdW interactions (see Table 1) indicating that the molecule is physisorbed; for ethylene, the vdW contributions to the overall binding energy (−0.97 eV at the optB86b-vdW level of theory) is ∼0.2 eV. Dispersion corrected calculations were not carried out for the aromatics; however, based on the observations for sulfur- and nitrogen-containing compounds, we can expect stabilizations of 0.5–0.6 eV for benzene and toluene and close to 1 eV for naphthalene.

We also did not explicitly study the effect of vdW corrections for alkyl substituted acridines, dimethyl pyrrole, dimethyl carbazole, and benzocarbazole. For these compounds, the effect of dispersion interactions is expected to be similar to that of their parent compounds (viz. acridine, pyrrole, and carbazole, respectively). Further, given the computational demands of such a study, we did not study the vdW-corrected differential binding energy values of organonitrogen compounds at varying surface concentrations. We, however, expect two competing factors in this case: (a) destabilization

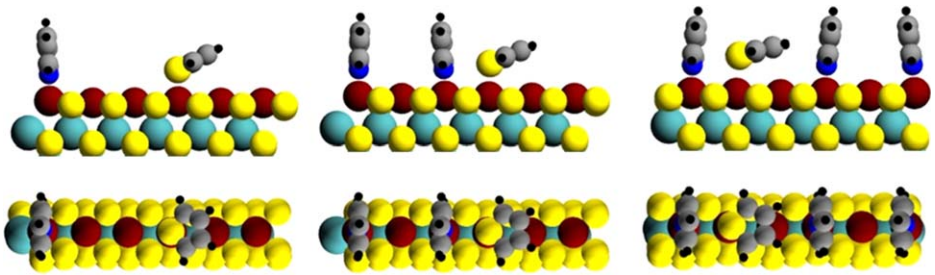

Figure 8. Most stable adsorption structure (GGA-PW91) of thiophene in the presence of one (left), two (center), and three (right) molecules of pyridine on NiMoS.

Red: nickel, yellow: sulfur, cyan: molybdenum, black: hydrogen, gray: carbon, and blue: nitrogen. [Color figure can be viewed in the online issue, which is available at wileyonlinelibrary.com.]

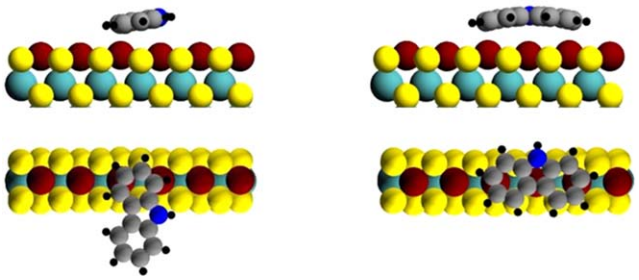

Figure 10. Most stable adsorption structure of carbazole on NiMoS: GGA-PW91 (left) and van der Waals corrected optB86b-vdW (right).

Red: nickel, yellow: sulfur, cyan: molybdenum, black: hydrogen, gray: carbon, and blue: nitrogen. [Color figure can be viewed in the online issue, which is available at wileyonlinelibrary.com.]

as observed for GGA-PW91 calculations, and (b) adsorbate-adsorbate attractive dispersion interactions. The net effect of these factors is expected to lead to a more gradual decrease in differential binding energies of adsorbate at higher surface concentrations compared to using only semilocal functionals (such as GGA-PW91).

Coadsorbed Thiophene and Organonitrogen Compounds. Destabilization in thiophene adsorption due to the presence of preadsorbed organonitrogen compounds was calculated taking into account vdW interactions. Table 4 contains the vdW-corrected destabilization energies ($D_{\text{Thiophene}}$) for the case of one nitrogen-containing molecule preadsorbed in the supercell. $D_{\text{Thiophene}}$ increases with the size of the preadsorbed nitrogen-containing molecule, from 0.2 eV for ammonia to about 0.5 eV for acridine and carbazole. Further, the adsorption structure of thiophene remains the same as that obtained at the GGA-PW91 level of theory (and hence similar to those

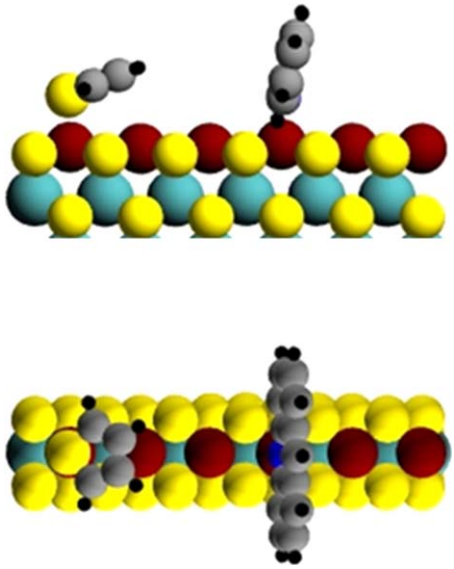

Figure 11. Most stable adsorption structure of thiophene in the presence of one preadsorbed molecule of acridine (vdW corrections included).

Red: nickel, yellow: sulfur, cyan: molybdenum, black: hydrogen, gray: carbon, and blue: nitrogen. [Color figure can be viewed in the online issue, which is available at wileyonlinelibrary.com.]

Table 4. Destabilization Energy of Thiophene Adsorption due to the Preadsorption of One Nitrogen-Containing Molecule in the Supercell at optB86b-vdW Level of Theory

Compound	$D_{\text{Thiophene}}$ (eV)
Ammonia	0.22
Pyridine	0.22
Aniline	0.26
Lutidine	0.40
Indole	0.42
Quinoline	0.39
Acridine	0.53
Carbazole	0.47

obtained at optB86b-vdW on a clean edge); for nitrogen-containing compounds, the adsorption structures are similar to that obtained for individual adsorption at the optB86b-vdW level of theory except for acridine which in the presence of thiophene prefers to adsorb in a perpendicular and upright configuration (Figure 11); this structure is also the most stable for coadsorption evaluated at GGA-PW91 level of theory.

Inhibition constants: Experiments vs. theory

Several studies have reported parameters for inhibition of HDS on NiMoS, due to adsorption of organonitrogen compounds. Specifically, La Vopa and Satterfield[39] studied the inhibition effects of several nitrogen-containing compounds on the HDS of thiophene on NiMoS at 633 K and 70 atm. They found that: (a) the rate of HDS of thiophene is first order with respect to thiophene, (b) inhibition of HDS by these nitrogen-containing compounds can approximately be modeled using Langmuir–Hinshelwood models, and (c) the nitrogen compounds are relatively unreactive as compared to thiophene. Similar studies have been reported by Nagai et al.,[40] Beltramone et al.,[60] and Prins and Egorova.[42]

Table 5 lists the experimental inhibition constants reported by La Vopa and Satterfield[39] and Nagai et al.[40] The order of magnitude of these numbers are close to each other although Nagai et al. reports values for inhibition of hydrogenation of dibenzothiophene; the value reported by Egorova and Prins[42] for inhibition of dibenzothiophene HDS by 2-methyl pyridine (0.53 kPa^{-1}) and that estimated by Raghuveer et al.[61] through kinetic modeling of pyridine HDN (61 atm^{-1}) is also consistent with pyridine values shown in Table 5 (noting that single methyl substitution does not lead to steric hindrance in pyridine based on our calculations). However, these values are two orders of magnitude smaller than that reported by Beltramone et al.[60]; the origin of these differences is unclear. However, because three of the four independent works are mutually consistent, we take the data in Table 5 for comparison. The adsorption equilibrium constants, based on the GGA-PW91 and vdW-corrected calculated binding energies, are also given in Table 5 for 633 K. The Supporting Information includes the enthalpy and entropy of adsorption values for these molecules and a discussion of the method used to calculate them (Supporting Information S5 and S6).

The equilibrium adsorption constants obtained at the GGA-PW91 level of theory significantly underpredict experimental inhibition constants for most molecules except for ammonia. The inclusion of vdW interactions reduces this experiment/theory discrepancy considerably; this, however, leads to overprediction of the equilibrium adsorption constant for ammonia and pyridine and underprediction for larger molecules. For aniline, quinoline, and carbazole, though $\Delta(\Delta G)$ is positive

Table 5. Experimental Values for Inhibition Constants (atm^{-1}), Calculated GGA-PW91 and vdW-Corrected (optB86b) Equilibrium Constants (atm^{-1}), and the Difference $\Delta(\Delta G)$ between the vdW-Corrected Calculated Values and the Experimental Values Reported by La Vopa et al.[39] or Nagai et al.[40] (for Acridine) on a Free Energy Basis: Negative Values in $\Delta(\Delta G)$ Imply Overpredictions

	Experimental Data				
Compound	La Vopa[39]	Nagai[40]	GGA-PW91	optB86b-vdW	$\Delta(\Delta G)$[a] (eV)
Ammonia	4.86		30.73	295.96	−0.22
Aniline	9.52	19	1.76×10^{-5}	0.15	0.23
Pyridine	43.6	107	0.18	101.19	−0.05
Lutidine	11.1		1.13×10^{-5}	0.05	0.30
Quinoline	99.3	131	2.20×10^{-5}	7.4×10^{-3}	0.43
Carbazole	51.6		4.65×10^{-10}	0.18	0.44
Acridine		200	3.32×10^{-7}	0.13	0.40

[a]Comparison is always between optB86b-vdW and experimental data by La Vopa et al. except for acridine where the comparison is with Nagai et al.

(underprediction), the discrepancy can be partially accounted for by the errors (~ 20–30 J/mol K overprediction) in calculated gas-phase entropy compared with experimental data (see Supporting Information S5 for details). For acridine, our comparison is with the data from Nagai et al.[40]; it should be reemphasized that the experimentally reported values are for inhibition of the hydrogenation step of dibenzothiophene (not HDS *per se*) and are consistently higher than that reported by La Vopa and Sattefield.[39]

Discussion

Factors governing adsorption

The binding energy of compounds relevant in hydrotreating processes depends on a number of factors including molecular size, basicity, resonance stabilization, electron density, and steric hindrance by substituents. Basic nitrogen-containing compounds and, in general, those containing high electron density (including olefins) adsorb more strongly on NiMoS than nonbasic nitrogen containing compounds, alkanes, and aromatic compounds wherein the electron density is lower or delocalized. Further, preferred adsorbed structures involve the interaction of a center of electron density—an atom containing a lone pair, a π or an aromatic bond, and so forth—directly with nickel atoms. The square planar geometry of the nickel edge allows for direct adsorption. The brim of the catalyst does not offer the most stable adsorption sites on NiMoS, in contrast to scanning tunneling microscopy (STM) and DFT studies on the adsorption of organonitrogen and organosulfur compounds on unpromoted and Co-promoted edges[25,62–64] that show adsorption to be favored on the brim sites of CoMoS.

A Bader charge analysis (details in Supporting Information S11) showed that there is electronic charge transfer from the adsorbates to the nickel atoms on the edge. In particular, the charge density difference plots for upright-perpendicular adsorption of pyridine and lutidine are given in Supporting Information S12. The binding of these nitrogen-containing compounds on NiMoS, therefore, is akin to Lewis acid-base complexation. To further test this hypothesis, we evaluated the gas-phase GGA-PW91 complexation energy of several nitrogen-containing compounds with aluminum chloride ($AlCl_3$) monomer—a representative Lewis acid—and compared these values with the corresponding GGA-PW91 binding energy values on NiMoS (Figure 12). The definition and values of complexation energy and comparison of GGA-PW91 with higher level gas-phase quantum mechanical theory calculations are given in Supporting Information S10. The binding energy values of basic and nonbasic organonitrogen compounds follow disparate but linear trends with the complexation energy; the slope for the basic compounds (green solid circles in Figure 12) is 1.0 while that for nonbasic (blue squares in Figure 12) is 0.6 and the respective mean absolute errors are 0.09 and 0.04 eV. The structures used for complexation energy calculations mimic that of adsorption on the NiMoS edge in that the complexation with aluminum chloride is via the nitrogen or carbon atom as the case may be for adsorption on NiMoS. The relative order of stability of different adsorbate orientations on the NiMoS edge were further found to be preserved for the complexation with aluminum chloride. The plot in Figure 12 includes basic compounds that prefer to bind via the aromatic ring (dimethyl acridine and dimethyl quinoline); these points lie very close to the nonbasic trend line (open circles in Figure 12). Interestingly, the binding energy values corresponding to their upright-perpendicular adsorption through nitrogen follow the trend of other basic compounds.

Effect of alkyl substitution

The presence of methyl groups on basic nitrogen compounds can affect the binding energy on NiMoS relative to the

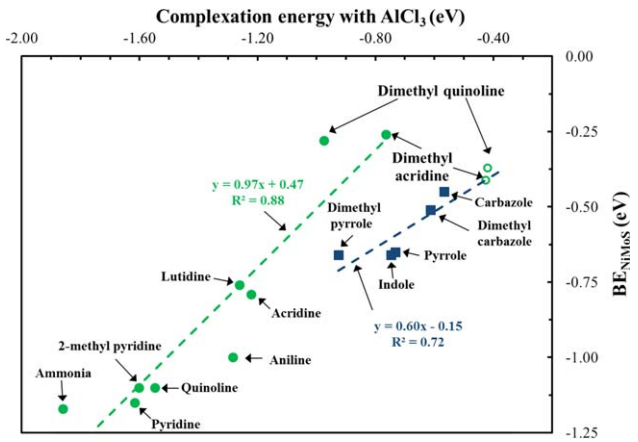

Figure 12. Binding energy of nitrogen-containing compounds on NiMoS vs. complexation energy with $AlCl_3$ (g).

Green circles and blue squares correspond to basic and nonbasic compounds, respectively; filled and open circles correspond to binding via the nitrogen atom and aromatic ring, respectively. The binding and complexation energy data are given in Supporting Information S10. [Color figure can be viewed in the online issue, which is available at wileyonlinelibrary.com.]

unsubstituted compound. Monomethyl substitution at a position closest to nitrogen does not affect the adsorption of small molecules such as 2-methyl pyridine which tilts slightly perpendicular to the edge to accommodate the methyl group; for larger molecules such as acridine, the presence of even a single methyl substitution at a position closest to nitrogen (4-methyl) changes the adsorption mode to a flat adsorption structure interacting through the aromatic ring (such as in the case of 4-methyl acridine). In general, methyl substitutions that do not sterically hinder the adsorption through the nitrogen atom in a basic compound do not affect the binding energy or structure. Dialkyl substitutions at the closest possible positions to the nitrogen atom of the molecule significantly affect adsorption irrespective of the size of the alkyl chain (e.g., lutidine and dialkyl acridine with respect to pyridine and acridine, respectively). While the Ni—N bond distance in lutidine increases relative to pyridine, and the perpendicular adsorption mode is still the most stable, dimethyl quinoline and dimethyl acridine prefer to adsorb flat and parallel similar to nonbasic compounds in contrast to quinoline and acridine. For nonbasic heteroaromatic compounds such as carbazole and aromatics such as benzene, on the other hand, methyl substitution leads to slight increase in binding strength. In general, therefore, alkyl substitution can lead to significant steric hindrance if the preferred adsorption is through the nitrogen atom; the effect of substitution is negligible or mildly beneficial for flat adsorption mode through the aromatic ring.

Effect of dispersion corrections

The vdW dispersion interactions are significant for large nitrogen-containing compounds such as acridine and carbazole which experience a net stabilization of $\sim$1 eV. For both compounds, the most stable adsorption structure with optB86b-vdW is the flat-parallel mode, rather than the perpendicular configuration (upright for acridine and flat for carbazole) identified using the GGA-PW91 functional. For larger molecules, such as benzoacridine and benzocarbazole, which are also present in crude fractions, the vdW interactions will dominate over electronic interactions and the flat-parallel adsorption mode will likely be the most stable. vdW interactions are also significant for organosulfur compounds; however, per our calculations, they do not alter the binding modes significantly. A flat-parallel adsorption structure for 4,6 dimethyldibenzothiophene is only 0.05 eV less favorable than the most stable structure (shown in Figure 6) and can be considered iso-energetic to within the accuracy of DFT. Parallel and flat (or slanted) adsorption modes typically have a higher vibrational entropy than upright-perpendicular structures per our calculations; consequently, the entropy change due to adsorption for parallel and flat adsorption modes is lower than upright-perpendicular modes by about 5 J/mol K. For 4,6-dimethyldibenzothiophene, this difference could stabilize the flat and parallel structure vis-à-vis the perpendicular structure.

Inhibition effect of nitrogen-containing compounds

Upon the inclusion of vdW corrections in our calculations, we note that both basic and nonbasic compounds adsorb more strongly than thiophene and that larger nitrogen compounds can compete with substituted dibenzothiophenes. This is particularly significant for nonbasic compounds such as carbazole and indole which would not be considered likely inhibitors of dibenzothiophene HDS based on simple GGA-PW91 calculations. As discussed earlier in Introduction, several experimental studies have shown that HDS is affected by basic and nonbasic organonitrogen compounds, however, the mode of inhibition is still unclear. Adsorption constants calculated in this study tend to overpredict experimental inhibition constant values for small molecules while underpredicting those constants for larger molecules. The inhibition constants obtained from La Vopa and Satterfield[39] represent apparent adsorption constants (K_{app}) and are, in general, different from the intrinsic adsorption constants (K_{int}) that are calculated here using DFT. Equation 10 describes the relationship between K_{app} and K_{int} at high coverage, assuming that the transition state of the HDS rate-determining step is destabilized to the same extent as thiophene adsorption. The detailed derivation is given in Supporting Information S7

$$K_{int}e^{\left(\frac{D_{Thiophene}}{RT}\right)}=K_{app} \tag{10}$$

The intrinsic adsorption constant and the destabilization energy are both functions of n, the number of adsorbed molecules on the edge. As n increases, K_{int} tends to decrease while $D_{Thiophene}$ increases. We can write K_{int} as a function of n as

$$K_{int}=K_{int}(n)=K_{int}(1)e^{\left(\frac{-\Delta E_{net,n}}{RT}\right)} \tag{11}$$

assuming that the entropy change of adsorption is constant. $K_{int}(1)$ is the optB86b-vdW adsorption constant reported in Table 5. The difference between intrinsic and apparent adsorption constants, therefore, depends on $D_{Thiophene,n}-\Delta E_{net,n}$. For $n=1$, $\Delta E_{net,n}$ is zero by definition, and the difference between intrinsic and apparent adsorption constants is determined by the destabilization energy reported in Tables 2 and 3. For larger compounds, such as carbazole and acridine, the destabilization energy corrects for the difference values $\Delta(\Delta G)$ reported in Table 5 (considering the optB86b-vdW value). For ammonia, on the other hand, we note that the gap between the intrinsic and apparent adsorption constants reduces for $n\geq 2$ using the values in Table 3 and assuming negligible differences in the value of $D_{Thiophene}$ in the presence of ammonia calculated using optB86b-vdW and GGA-PW91. Although approximate, this analysis suggests that large organonitrogen compounds inhibit HDS even at low surface concentration ($n=1$) through destabilization while small molecules such as ammonia tend to adsorb at high concentrations ($n\geq 2$). Nevertheless, in all cases, the inhibition is due to (1) blocking of potential HDS sites, and (2) destabilization of HDS intermediates and HDS relevant transition states by nitrogen-containing adsorbates.

Inhibition by hydrocarbons

The products of HDS and HDN are hydrocarbons comprising of substituted aromatics, naphthenics, alkanes, and olefins. Our calculations suggest that aromatics and olefins have a significant binding energy owing to their electron density. Further, based on our analysis of the organonitrogen and organosulfur compounds, we can expect a significant stabilization of aromatics by vdW interactions. Alkanes, on the other hand, interact only via vdW interactions. The nature of the reactant molecule and the level of hydrogenation will, therefore, determine the level of inhibition by products of HDS.

Comparison with experiments

The adsorption structure potentially affects the reactivity and the dominant reaction pathways of heteroatom removal processes—HDS of organosulfur and HDN of organonitrogen

compounds. We can, therefore, relate dominant pathways with adsorption structure and compare this with our predictions. For example, it is known that dibenzothiophene undergoes direct desulfurization predominantly wherein the sulfur atom is directly removed leading to biphenyl as the major product. In contrast, 4,6-dimethyl dibenzothiophene prefers the hydrogenation pathway involving the hydrogenation of one of its aromatic rings leading to substituted cyclohexyl benzene as the major product.[37] This has been rationalized in terms of the adsorption structures of the reactants and steric hindrance of 4,6-dimethyl dibenzothiophene. Our discussion earlier is consistent with this argument—dibenzothiophene adsorbs via the sulfur atom while 4,6-dimethyl dibenzothiophene can adsorb through its aromatic rings in a flat and parallel configuration. Further, organonitrogen compounds inhibit the hydrogenation pathway in HDS of dibenzothiophenes significantly.[35,42,65] This can be rationalized, again, on the basis of the calculated adsorption structure. The hydrogenation pathway requires the flat-parallel adsorption structure which is likely destabilized to a greater extent by the presence of these organonitrogen compounds, some of which themselves tend to adsorb in a flat-parallel adsorption structure. As a result, the hydrogenation pathway is significantly inhibited.

Similar observations and comparisons can be made for HDN of organonitrogen compounds. HDN of pyridine, quinoline, and acridine involves the hydrogenation of the heteroaromatic ring.[66,67] For pyridine and quinoline, this is in line with the upright adsorption structure; for acridine, however, the parallel and flat adsorption structure identified upon including vdW corrections is inconsistent with that observation because, at 633 K, the adsorption free energy of the flat-parallel structure was calculated to be more stable than the upright-perpendicular one by 0.2 eV. There are two explanations for this discrepancy. First, although the adsorption constant is lower for the perpendicular upright structure, the activation of the heteroaromatic ring could be easier than that of the aromatic ring. Second, under these conditions, concentration of adsorbed acridine could be higher than that considered in this work, that is, $n > 1$ wherein the adsorption configuration could be significantly different from the flat and parallel configuration obtained upon including vdW interactions. HDN of indole has been shown to follow the hydrogenation route wherein both rings are hydrogenated first prior to C—N bond scission.[68] This is consistent with our result that indole adsorbs flat and parallel allowing for hydrogenation of its rings.

The effect of alkyl substitution can also be inferred from experimental studies and compared with our results. For substituted quinoline, it was shown that methyl groups on the heteroaromatic ring reduce HDN activity on NiMoS.[69] This is consistent with our observations that methyl groups sterically hinder adsorption via the nitrogen atom. Conversely, methyl substitutions on closest available carbon atoms of indole (2- and 7-methyl indole), do not affect HDN conversion on NiMoS.[70] This is also consistent with a flat and parallel adsorption structure which shows minimal steric hindrance. Further, the inclusion methyl substituents in the benzene ring of indole increases hydrogenation rates, in line with our results that methyl groups have a slight beneficial effect on binding as observed for substitutions in carbazole and benzene. La Vopa and Satterfield[39] show that lutidine inhibits HDS to a lesser extent than pyridine, consistent with our calculations of binding energy and adsorption constants.

Future scope of study

Our analysis of adsorption of nitrogen-containing compounds can predict and account for several experimental trends as discussed above; however, this work does not take into consideration several factors that could play a significant role in HDS and HDN. These are discussed below for detailed consideration in the future.

First, we did not consider the adsorption of and destabilization by HDN intermediates on NiMoS. Although La Vopa and Satterfield[39] report that while HDN conversion was negligible under their conditions, some of the organonitrogen compounds such as quinoline equilibrated with their hydrogenated counterparts. Further, under realistic conditions with realistic feedstocks containing larger organosulfur compounds, there is significant HDN resulting in an appreciable amount of ammonia in the effluent streams of hydrotreaters.[71] As a preliminary test, we show in Supporting Information S13 how simple intermediates, specifically monohydrogenated forms of some of the molecules studied so far—ammonia, pyrrole, and pyridine—adsorb on NiMoS. We find that ammonium (NH_4) prefers to adsorb on the brim sulfur atoms of NiMoS as opposed to directly on the Ni atoms; however, the hydrogenation of adsorbed ammonia by stoichiometric amounts of H_2 (gas) to form ammonium is endothermic by about 0.1 eV at GGA-PW91 level of theory. For monohydrogenated pyrrole intermediates (two likely intermediates were studied: 2- and 3-hydropyrrole), the hydrogenation of adsorbed pyrrole by H_2 (gas) is exothermic (~ -0.2 eV for 3-hydropyrrole) or mildly endothermic (less than 0.05 eV) at GGA-PW91 for 2-hydropyrrole and the adsorption is flat on the edge atop two adjacent nickel atoms in both cases. For hydrogenated pyridine, N-hydrogenation (1-hydropyridine) and C-2-hydrogenation (2-hydropyridine) were considered; hydrogenation was endothermic (>0.3 eV at GGA-PW91) in both cases and the adsorption was also flat and atop two adjacent nickel atoms in contrast to adsorption of pyridine which prefers an upright and perpendicular configuration.

Second, alternative sites need to be further explored. For example, nickel atoms can also promote the sulfur edges, not just the metal edges. Indeed, the Ni:(Ni+Mo) ratio of the catalysts used by La Vopa and Satterfield,[39] Nagai et al.,[40] and Beltramone et al.[60] is between 0.25 and 0.35. For such ratios, nickel atoms can also occupy the sulfur edge. Indeed, STM studies also show nickel promoting the sulfur edge.[29] The nickel promoted sulfur edge is, therefore, an important alternative active site location. Further, it has been recently shown through STM that dibenzothiophene can adsorb at the corners of unpromoted molybdenum sulfide catalyst particles.[64] Such sites are, therefore, likely sites for inhibition by nitrogen compounds as well. In addition, Lercher and coworkers[35] showed that the IR spectra of CO adsorption on $NiMoS/Al_2O_3$ shows several bands corresponding to multiple types of sites, including Ni sites, Mo sites, and Mo sites that are in the vicinity of nickel atoms. In particular, they correlated the HDN activity of the catalyst with the proportion of nonpromoted edge of catalyst particles over various supports; the fraction of nonpromoted edge is about 0.27 according to their calculations. This implies the partial promotion such as that discussed by Raybaud and coworkers.[31,47]

Third, although we calculated the effect of the second slab on adsorption, we do not consider the effect of support which can lead to significant electronic and possibly dispersion interactions.[34,36] Specifically, the orientation of the catalyst particle

relative to the support and the nature of its interaction with the support (presence/absence of chemical bonds between molybdenum atoms of the catalyst and oxygen atoms of the support) can affect the chemisorption of adsorbates on the catalyst edges; the adsorption on the edges of the catalyst can also be further stabilized due to dispersion interactions with the support. Inclusion of the support, however, will significantly increase the computational cost of calculations. Relatedly, we have not considered the effect of the second slab when accounting for vdW dispersion; while a perpendicular adsorption can be hindered by the proximity of the second slab (as discussed in Results Section), a higher level of dispersion interaction between the ends of the adsorbate and the second slab is possible, thereby stabilizing the configuration.

Conclusions

Adsorption of nitrogen-containing compounds, sulfur-containing compounds, hydrocarbons, and small molecules such as hydrogen, hydrogen sulfide, and ammonia on the metal edge of NiMoS was studied using plane wave periodic density functional theory accounting for vdW interactions. We find that: (a) adsorbates prefer the Ni-promoted edge over the brim, (b) per GGA-PW91, basic nitrogen-containing compounds adsorb stronger than nonbasic ones, but both adsorb directly on top of the nickel atom, (c) basic compounds tend to adsorb via nitrogen atoms in an upright and perpendicular configuration with respect to the edge while nonbasic compounds via the carbon atoms or the aromatic ring in a flat/slanted configuration, parallel or perpendicular to the edge, (d) the binding of organonitrogen compounds on the NiMoS metal edge mimics Lewis acid-base complexation, and (e) vdW interactions are significant, specifically for larger molecules such as acridine and carbazole (net stabilization of 0.7 and 1.0 eV, respectively), the most stable adsorption structures of which are found to be flat and parallel to the nickel edge, allowing for the maximum interaction of the carbon and nitrogen atoms with the edge. We also calculated the temperature-corrected enthalpy and entropy of adsorption of these compounds and found that the adsorption constants match experimental inhibition constants of organonitrogen compounds on thiophene HDS to within 0.3 eV in free energy terms. Specifically, we overpredict for the case of small basic compounds such as ammonia and underpredict for larger compounds such as acridine and carbazole. This discrepancy can be accounted for on the basis of coverage effects and destabilization of thiophene adsorption in the presence of nitrogen-containing compounds on the edge. We, therefore, suggest that inhibition by nitrogen-containing compounds can be due to both site blocking (or poisoning) and destabilization of HDS reaction intermediates and related transition states.

Acknowledgments

The authors acknowledge financial support from BP Products North America Inc. and specifically thank Drs. Hong Yang, Corneliu Buda, Dong Wang, and Phil Sinclair for valuable discussions during the course of this work. The computational work was performed partly using supercomputing resources at EMSL, a national scientific user facility at Pacific Northwest National Lab (PNNL), the Center for Nanoscale Materials (CNM) at Argonne National Lab (ANL), the UW-Madison Center for High Throughput Computing (CHTC) in the Department of Computer Science, and the National Energy Research Scientific Computing center (NERSC). EMSL is sponsored by the Department of Energy's Office of Biological and Environmental Research located at PNNL. CNM and NERSC are supported by the U.S. Department of Energy, Office of Science, under contracts DE-AC02-06CH11357 and DE-AC02-05CH11231, respectively. The CHTC is supported by UW-Madison, the Advanced Computing Initiative, the Wisconsin Alumni Research Foundation, the Wisconsin Institute for Discovery, and the National Science Foundation, and is an active member of the Open Science Grid, which is supported by the National Science Foundation and the U.S. Department of Energy's Office of Science.

Literature Cited

1. Stanislaus A, Marafi A, Rana MS. Recent advances in the science and technology of ultra low sulfur diesel (ULSD) production. *Catal Today*. 2010;153(1–2):1–68.
2. Ho TC. Deep HDS of diesel fuel: chemistry and catalysis. *Catal Today*. 2004;98(1–2):3–18.
3. Topsoe H. The role of Co-Mo-S type structures in hydrotreating catalysts. *Appl Catal A Gen*. 2007;322:3–8.
4. Houssenbay S, Kasztelan S, Toulhoat H, Bonnelle JP, Grimblot J. Nature of the different nickel species in sulfided bulk and alumina-supported NiMo hydrotreating catalysts. *J Phys Chem*. 1989;93(20):7176–7180.
5. Delannay F. High-resolution electron-microscopy of hydrodesulfurization catalysts. *Appl Catal*. 1985;16(2):135–152.
6. Topsoe NY, Topsoe H. Characterization of the structures and active-sites in sulfided $CoMo/Al_2O_3$ catalysts by NO chemisorption. *J Catal*. 1983;84(2):386–401.
7. Bouwens S, Koningsberger DC, Debeer VHJ, Louwers SPA, Prins R. EXAFS study of the local-structure of Ni in Ni-MoS_2/C hydrodesulfurization catalysts. *Catal Lett*. 1990;5(3):273–284.
8. Raybaud P. Understanding and predicting improved sulfide catalysts: insights from first principles modeling. *Appl Catal A Gen*. 2007;322:76–91.
9. Sun MY, Adjaye J, Nelson AE. Theoretical investigations of the structures and properties of molybdenum-based sulfide catalysts. *Appl Catal A Gen*. 2004;263(2):131–143.
10. Hinnemann B, Moses PG, Norskov JK. Recent density functional studies of hydrodesulfurization catalysts: insight into structure and mechanism. *J Phys Condens Matter*. 2008;20(6):064236.
11. Topsoe H, Clausen BS. Active-sites and support effects in hydrodesulfurization catalysts. *Appl Catal*. 1986;25(1–2):273–293.
12. Besenbacher F, Brorson M, Clausen BS, Helveg S, Hinnemann B, Kibsgaard J, Lauritsen JV, Moses PG, Nørskov JK, Topsøe H. Recent STM, DFT and HAADF-STEM studies of sulfide-based hydrotreating catalysts: insight into mechanistic, structural and particle size effects. *Catal Today*. 2008;130(1):86–96.
13. Daage M, Chianelli RR. Structure-function relations in molybdenum sulfide catalysts - the rim-edge model. *J Catal*. 1994;149(2):414–427.
14. Kasztelan S, Toulhoat H, Grimblot J, Bonnelle JP. A geometrical model of the active phase of hydrotreating catalysts. *Appl Catal*. 1984;13(1):127–159.
15. Bataille F, Lemberton JL, Michaud P, Perot G, Vrinat, M, Lemaire M, Schulz E, Breysse M, Kasztelan S. Alkyldibenzothiophenes hydrodesulfurization-promoter effect, reactivity, and reaction mechanism. *J Catal*. 2000;191(2):409–422.
16. Cristol S, Paul JF, Payen E, Bougeard D, Clemendot S, Hutschka F. Theoretical study of the MoS_2 (100) surface: a chemical potential analysis of sulfur and hydrogen coverage. *J Phys Chem B*. 2000;104(47):11220–11229.
17. Cristol S, Paul JF, Payen E, Bougeard D, Clemendot S, Hutschka F. Theoretical study of the MoS_2 (100) surface: a chemical potential analysis of sulfur and hydrogen coverage. 2. Effect of the total pressure on surface stability. *J Phys Chem B*. 2002;106(22):5659–5667.
18. Travert A, Nakamura H, van Santen RA, Cristol S, Paul JF, Payen E. Hydrogen activation on Mo-based sulfide catalysts, a periodic DFT study. *J Am Chem Soc*. 2002;124(24):7084–7095.

19. Paul JF, Payen E. Vacancy formation on MoS_2 hydrodesulfurization catalyst: DFT study of the mechanism. *J Phys Chem B*. 2003; 107(17):4057–4064.
20. Schweiger H, Raybaud P, Kresse G, Toulhoat H. Shape and edge sites modifications of MoS_2 catalytic nanoparticles induced by working conditions: a theoretical study. *J Catal*. 2002;207(1):76–87.
21. Prodhomme P-Y, Raybaud P, Toulhoat H. Free-energy profiles along reduction pathways of MoS_2 M-edge and S-edge by dihydrogen: a first-principles study. *J Catal*. 2011;280(2):178–195.
22. Byskov LS, Bollinger M, Nørskov JK, Clausen BS, Topsøe H. Molecular aspects of the H-2 activation on MoS_2 based catalysts the role of dynamic surface arrangements. *J Mol Catal A Chem*. 2000; 163(1–2):117–122.
23. Bollinger MV, Jacobsen KW, Nørskov JK. Atomic and electronic structure of MoS_2 nanoparticles. *Phys Rev B*. 2003;67(8):085410.
24. Raybaud P, Hafner J, Kresse G, Kasztelan S, Toulhoat H. Structure, energetics, and electronic properties of the surface of a promoted MoS_2 catalyst: an ab initio local density functional study. *J Catal*. 2000;190(1):128–143.
25. Lauritsen JV, Bollinger MV, Laegsgaard E, Jacobsen KW, Nørskov JK, Clausen BS, Topsøe H, Bensenbacher F. Atomic-scale insight into structure and morphology changes of MoS_2 nanoclusters in hydrotreating catalysts. *J Catal*. 2004;221(2):510–522.
26. Hensen EJM, Kooyman PJ, van der Meer Y, van der Kraan AM, de Beer VHJ, van Veen JAR, van Santen RA. The relation between morphology and hydrotreating activity for supported MoS_2 particles. *J Catal*. 2001;199(2):224–235.
27. Berhault G, De la Rosa MP, Mehta A, Yacaman MJ, Chianelli RR. The single-layered morphology of supported MoS_2-based catalysts - the role of the cobalt promoter and its effects in the hydrodesulfurization of dibenzothiophene. *Appl Catal A Gen*. 2008;345(1):80–88.
28. Topsoe H, Hinnemann B, Nørskov JK, Lauritsen JV, Besenbacher F, Hansen PL, Hytoft G, Egeberg RG, Knudsen KG. The role of reaction pathways and support interactions in the development of high activity hydrotreating catalysts. *Catal Today*. 2005;107–108:12–22.
29. Lauritsen JV, Kibsgaard J, Olesen GH, Moses PG, Hinnemann B, Helveg S, Nørskov JK, Clausen, BS, Topsøe H, Laegsgaard E, Besenbacher, F. Location and coordination of promoter atoms in Co- and Ni-promoted MoS(2)-based hydrotreating catalysts. *J Catal*. 2007;249(2):220–233.
30. Schweiger H, Raybaud P, Toulhoat H. Promoter sensitive shapes of Co(Ni)MoS nanocatalysts in sulfo-reductive conditions. *J Catal*. 2002;212(1):33–38.
31. Krebs E, Silvi B, Raybaud P. Mixed sites and promoter segregation: a DFT study of the manifestation of Le Chatelier's principle for the Co(Ni)MoS active phase in reaction conditions. *Catal Today*. 2008; 130(1):160–169.
32. Sun MY, Nelson AE, Adjaye J. On the incorporation of nickel and cobalt into MoS_2-edge structures. *J Catal*. 2004;226(1):32–40.
33. Kibsgaard J, Lauritsen JV, Laegsgaard E, Clausen BS, Topsoe H, Besenbacher F. Cluster-support interactions and morphology of MoS_2 nanoclusters in a graphite-supported hydrotreating model catalyst. *J Am Chem Soc*. 2006;128(42):13950–13958.
34. Costa D, Arrouvel C, Breysse M, Toulhoat H, Raybaud P. Edge wetting effects of gamma-Al_2O_3 and anatase-TiO_2 supports by MoS_2 and CoMoS active phases: a DFT study. *J Catal*. 2007;246(2):325–343.
35. Gutierrez OY, Singh S, Schachtl E, Kim J, Kondratieva E, Hein J, Lercher JA. Effects of the support on the performance and promotion of (Ni)MoS_2 catalysts for simultaneous hydrodenitrogenation and hydrodesulfurization. *ACS Catal*. 2014;4(5):1487–1499.
36. Hinnemann B, Norskov JK, Topsoe H. A density functional study of the chemical differences between type I and type II MOS_2-based structures in hydrotreating catalysts. *J Phys Chem B*. 2005;109(6): 2245–2253.
37. Prins R, Egorova A, Rothlisberger A, Zhao Y, Sivasankar N, Kukula P. Mechanisms of hydrodesulfurization land hydrodenitrogenation. *Catal Today*. 2006;111(1–2):84–93.
38. Furimsky E. Hydrodenitrogenation of petroleum. *Catal Rev Sci Eng*. 2005;47(3):297–489.
39. La Vopa V, Satterfield CN. Posioning of thiophene hydrodesulfurization by nitrogen-compounds. *J Catal*. 1988;110(2):375–387.
40. Nagai M, Sato T, Aiba A. Posioning effect of nitrogen-compounds on dibenzothiophene hydrodesulfurization on sulfided $NiMo/Al_2O_3$ catalysts and relation to gas-phase basicity. *J Catal*. 1986;97(1): 52–58.
41. Yang H, Chen JW, Fairbridge C, Briker Y, Zhu YJ, Ring Z. Inhibition of nitrogen compounds on the hydrodesulfurization of substituted dibenzothiophenes in light cycle oil. *Fuel Process Technol*. 2004;85(12):1415–1429.
42. Egorova M, Prins R. Mutual influence of the HDS of dibenzothiophene and HDN of 2-methylpyridine. *J Catal*. 2004;221(1):11–19.
43. Sun MY, Nelson AE, Adjaye J. First principles study of heavy oil organonitrogen adsorption on NiMoS hydrotreating catalysts. *Catal Today*. 2005;109(1–4):49–53.
44. Sun MY, Nelson AE, Adjaye J. Adsorption thermodynamics of sulfur- and nitrogen-containing molecules on NiMoS: a DFT study. *Catal Lett*. 2006;109(3–4):133–138.
45. Sun MY, Nelson AE, Adjaye J. Adsorption and hydrogenation of pyridine and pyrrole on NiMoS: an ab initio density-functional theory study. *J Catal*. 2005;231(1):223–231.
46. Qu LL, Zhang WP, Kooyman PJ, Prins R. MAS NMR, TPR, and TEM studies of the interaction of NiMo with alumina and silica-alumina supports. *J Catal*. 2003;215(1):7–13.
47. Krebs E, Daudin A, Raybaud P. A DFT study of CoMoS and NiMoS catalysts: from nano-crystallite morphology to selective hydrodesulfurization. *Oil Gas Sci Technol Rev D IFP Energies Nouv*. 2009;64(6):707–718.
48. Kresse G, Furthmuller J. Efficiency of ab-initio total energy calculations for metals and semiconductors using a plane-wave basis set. *Comput Mater Sci*. 1996;6(1):15–50.
49. Kresse G, Furthmuller J. Efficient iterative schemes for *ab initio* total-energy calculations using a plane-wave basis set. *Phys Rev B*. 1996;54(16):11169–11186.
50. Monkhorst HJ, Pack JD. Special points for brillouin-zone integrations. *Phys Rev B*. 1976;13(12):5188.
51. Kresse G, Joubert D. From ultrasoft pseudopotentials to the projector augmented-wave method. *Phys Rev B*. 1999;59(3):1758.
52. Perdew JP, Chevary JA, Vosko SH, Jackson KA, Pederson, MR, Singh DJ, Fiolhais C. Atoms, molecules, solids, and surfaces - applications of the generalized gradient approximation for exchange and correlation. *Phys Rev B*. 1992;46(11):6671–6687.
53. Perdew JP, Chevary JA, Vosko SH, Jackson KA, Pederson, MR, Singh DJ, Fiolhais C. Atoms, molecules, solids, and surfaces - applications of the generalized gradient approximation for exchange and correlation (Vol. 46, p. 6671, 1992) - erratum. *Phys Rev B*. 1993; 48(7):4978–4978.
54. Raybaud P, Kresse G, Hafner J, Toulhoat H. *Ab initio* density functional studies of transition-metal sulphides: I. Crystal structure and cohesive properties. *J Phys Condens Matter*. 1997;9(50):11085–11106.
55. Raybaud P, Hafner J, Kresse G, Toulhoat H. *Ab initio* density functional studies of transition-metal sulphides: II. Electronic structure. *J Phys Condens Matter*. 1997;9(50):11107–11140.
56. Klimes J, Bowler DR, Michaelides A. Van der Waals density functionals applied to solids. *Phys Rev B*. 2011;83(19):195131.
57. Klimes J, Bowler DR, Michaelides A. Chemical accuracy for the van der Waals density functional. *J Phys Condens Matter*. 2010; 22(2):022201.
58. McQuarrie DA. *Statistical Mechanics*. California: University Science Books, 2000.
59. Sun MY, Nelson AE, Adjaye J. Adsorption and dissociation of H_2 and H_2S on MoS_2 and NiMoS catalysts. *Catal Today*. 2005;105(1):36–43.
60. Beltramone AR, Crossley S, Resasco DE, Alvarez WE, Choudhary TV. Inhibition of the hydrogenation and hydrodesulfurization reactions by nitrogen compounds over NiMo/Al(2)O(3). *Catal Lett*. 2008;123(3–4):181–185.
61. Raghuveer CS, Thybaut JW, De Bruycker R, Metaxas K, Bera T, Marin GB. Pyridine hydrodenitrogenation over industrial NiMo/gamma-Al_2O_3 catalyst: application of gas phase kinetic models to liquid phase reactions. *Fuel*. 2014;125:206–218.
62. Moses PG, Hinnemann B, Topsoe H, Nørskov JK. The hydrogenation and direct desulfurization reaction pathway in thiophene hydrodesulfurization over MoS_2 catalysts at realistic conditions: a density functional study. *J Catal*. 2007;248(2):188–203.
63. Moses PG, Hinnemann B, Topsoe H, Nørskov JK. The effect of Co-promotion on MoS_2 catalysts for hydrodesulfurization of thiophene: a density functional study. *J Catal*. 2009;268(2):201–208.
64. Tuxen AK, Fuchtbauer HG, Temel B, Hinnemann B, Topsøe H, Knudsen KG, Besenbacher F, Lauritsen JV. Atomic-scale insight into adsorption of sterically hindered dibenzothiophenes on MoS_2 and Co-Mo-S hydrotreating catalysts. *J Catal*. 2012;295:146–154.
65. Egorova M, Prins R. Competitive hydrodesulfurization of 4,6-dimethyldibenzothiophene, hydrodenitrogenation of 2-methylpyridine, and

hydrogenation of naphthalene over sulfided NiMo/gamma-Al_2O_3. *J Catal*. 2004;224(2):278–287.
66. Girgis MJ, Gates BC. Reactivities, reaction networks, and kinetics in high-pressure catalytic hydroprocessing. *Ind Eng Chem Res*. 1991; 30(9):2021–2058.
67. Massoth FE, Kim SC. Kinetics of the HDN of quinoline under vapor-phase conditions. *Ind Eng Chem Res*. 2003;42(5):1011–1022.
68. Kim SC, Massoth FE. Kinetics of the hydrodenitrogenation of indole. *Ind Eng Chem Res*. 2000;39(6):1705–1712.
69. Kim SC, Simons J, Massoth FE. HDN activities of methyl-substituted quinolines. *J Catal*. 2002;212(2):201–206.
70. Kim SC, Massoth FE. Hydrodenitrogenation activities of methyl-substituted indoles. *J Catal*. 2000;189(1):70–78.
71. Choudhary TV, Gong K, Ellison P, Subbiah A. A glimpse into the molecular journey inside an ultralow sulfur diesel reactor. *ChemCatChem*. 2014;6(6):1782–1787.

Manuscript received May 28, 2015, and revision received Aug. 4, 2015.